IEEE Access
Multidisciplinary | Rapid Review | Open Access Journal

Received June 11, 2021, accepted June 27, 2021, date of publication June 29, 2021, date of current version July 12, 2021.

Digital Object Identifier 10.1109/ACCESS.2021.3093465

Frequency Coupling Admittance Modeling of Quasi-PR Controlled Inverter and Its Stability Comparative Analysis Under the Weak Grid

ZHIWEI XIE[1], YANDONG CHEN[1], (Senior Member, IEEE), WENHUA WU[1], (Member, IEEE), YICHAO WANG[1,2], WENLAN GONG[3], AND JOSEP M. GUERRERO[4], (Fellow, IEEE)

[1]National Engineering Research Center for Power Conversion and Control, Hunan University, Changsha 410082, China
[2]State Grid Hunan Electric Power Company Ltd., Economic and Technical Research Institute, Changsha 410007, China
[3]Electric Power Research Institute of Guangxi Power Grid Company Ltd., Nanning 530023, China
[4]Department of Energy Technology, Aalborg University, 9220 Aalborg, Denmark

Corresponding author: Yandong Chen (yandong_chen@hnu.edu.cn)

This work was supported in part by the National Key Research and Development Program of China under Grant 2017YFB0902000, in part by the National Science Foundation of China under Grant 52077070 and Grant 52007058, and in part by the Science and Technology Project of State Grid under Grant SGXJ0000KXJS1700841.

ABSTRACT This paper intends to comparatively study the stabilities of grid-connected inverters with three closely related controllers: quasi-proportional resonance (quasi-PR), proportional integral (PI), and proportional resonance (PR) under the weak grid. Firstly, considering the influence of frequency coupling characteristic, a frequency coupling admittance model of quasi-PR controlled inverter is established. Then, the admittance characteristics of the quasi-PR, PI and PR controlled inverters are compared. Admittance characteristics of the PI and PR controlled inverters are similar while the quasi-PR controlled inverter is quite different: the amplitude of the quasi-PR controlled inverter is larger than that of the PI controlled inverter and the phase difference between the two inverters is obvious in the mid-high frequency areas, which are mainly caused by the resonance bandwidth of the quasi-PR controller. Furthermore, the stabilities of the quasi-PR, PI and PR controlled inverters are analyzed. The stabilities of the PI and PR controlled inverters are similar but the quasi-PR controlled inverter is more sensitive to weak grid and high inverter output power. To achieve the same system stability, the voltage outer-loop bandwidth of the quasi-PR controlled inverter should be designed narrower than that of the PI and PR controlled inverters. Finally, experiments verify the correctness of the analyses.

INDEX TERMS Frequency coupling, admittance modeling, quasi-PR control, stability analysis.

I. INTRODUCTION

With the development of renewable energy generation, more and more power electronic converters are connected to the grid [1]–[3]. Inverters are used as the interface for renewable energy to connect to the grid, thus its control method has received a lot of attention [4], [5].

The PI control method in dq-domain (the synchronous reference frame) [6], [7], the PR and quasi-PR control methods in phase-domain (the stationary reference frame) [8], [9] are often used in the inner-loop control of grid-connected inverters. As a typical grid-connected inverter control method, the stability problem of the PI controlled inverter has been widely studied in [10], [11]. A small-signal transfer function model for the PI controlled inverter to analyze system stability has been established in [10] and the stability of the PI controlled inverter through the impedance-based method has been analyzed [11]. However, since the zero steady-state error performance of the PI control method should be achieved in dq-domain, several times of coordinate transformation are required during the control process [12]. Therefore, the conversion relationship between the control in dq-domain and the control in phase-domain is established, and the PR control method in phase-domain which is equivalent to the PI control method in dq-domain is proposed [13]. To reduce the sensitivity of

The associate editor coordinating the review of this manuscript and approving it for publication was Derek Abbott.

This work is licensed under a Creative Commons Attribution 4.0 License. For more information, see https://creativecommons.org/licenses/by/4.0/

the control system to slightly frequency deviation in the grid, quasi-PR control method, which is approximately equivalent to PR control method, is often applied in practice [14]. The quasi-PR control method has a relatively large gain at the fundamental frequency, which is helpful for the controller to nearly realize zero steady-state error performance. What's more, the quasi-PR control method can be directly used in phase-domain, which can reduce the times of coordinate transformation [15]. Therefore, the quasi-PR control method has attracted many attentions [17]–[21]. The effect of the quasi-PR controller gain on the control performance was analyzed [17], and an adaptive quasi-PR controller was proposed to obtain the controller parameters online when AC-side inductance is unknown [18]. An optimized design method was proposed in [19], which can effectively increase the proportional coefficient and integral coefficient gains of the quasi-PR controller. Quasi-PR controller is also applied to the control loops for sub-synchronous oscillation suppression of DFIG [20] and resonance suppression of the system while inverters are connected to the grid with the long transmission lines [21].

The PR control method in phase-domain can be derived from the PI control method in dq-domain, thus they can make the grid-connected inverters achieve a similar performance in different coordinate systems. However, the quasi-PR control method is obtained from the PR control method through introducing resonance bandwidth, which may change its control characteristics. It is worth to be studied whether the stability of the quasi-PR controlled inverter is consistent with that of the PR and PI controlled inverters. The sequence-impedance model of the quasi-PR and the PI controlled inverters was established in [22]. However, the built model does not consider the effects of the voltage outer-loop [23], [24] and the frequency coupling characteristic [25], which may lead to inaccurate analysis results. The effects of the PI control method in dq-domain and quasi-PR control method in phase-domain on the stability of the two-level VSC-HVDC system was compared in [26]. It pointed out that under the appropriate parameters, the PI controlled and the quasi-PR controlled systems have a similar dynamic performance. However, the above comparative analysis was performed when different control parameters were selected for the PI and quasi-PR controller without considering the relationship between these two control methods. Therefore, in this paper, considering the effects of voltage outer-loop, current inner-loop, phase-locked loop (PLL), control delay and frequency coupling characteristic, a frequency coupling admittance model of the quasi-PR controlled inverter is established, and the differences of the stability for the quasi-PR, PI and PR controlled inverters are explored under the same operating conditions.

The rest of the paper is organized as follows. In Section II, the relationship between the PI control method in dq-domain and the PR and quasi-PR control methods in phase-domain is introduced firstly. Then, the frequency coupling admittance model of the quasi-PR controlled inverter is built in Section III. The admittance characteristics of the quasi-PR, PI and PR controlled inverters are compared in Section IV, and the stabilities of the grid-connected inverters under these three control methods are analyzed through the impedance-based method and generalized Nyquist criterion in Section V. The experiments are carried out in Section VI. Finally, some conclusions are made in Section VII.

II. PI CONTROL METHOD IN DQ-DOMAIN AND QUASI-PR AND PR CONTROL METHODS IN PHASE-DOMAIN

Fig. 1(a) presents the topology of the grid-connected system, v_{dc} is the DC-side voltage; e_a, e_b and e_c are mid-point voltages of the grid-connected inverter; v_a, v_b, v_c, i_a, i_b and i_c are the output voltages and inductor currents of the grid-connected inverter; L_f, C_f and R_f are the filter inductor, capacitor, and damping resistance, respectively; L_g and R_g are the equivalent line inductance and resistance of the grid, respectively.

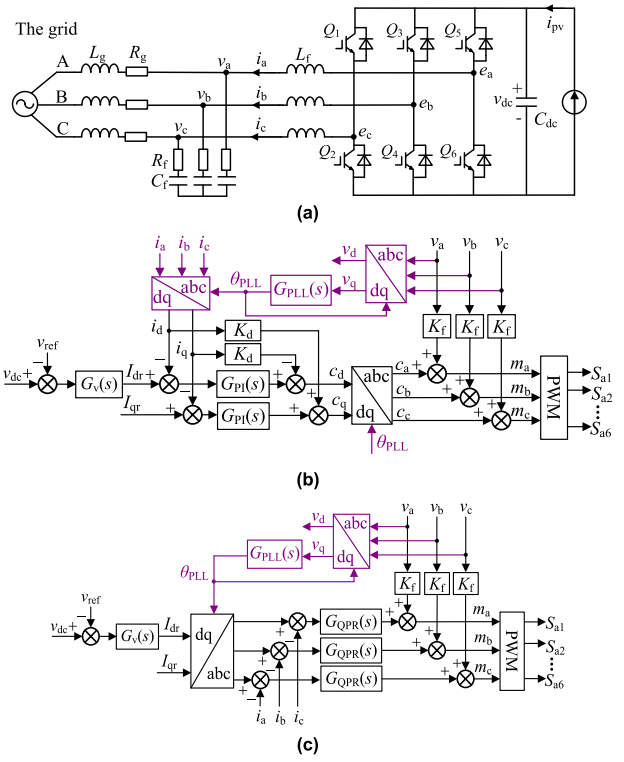

FIGURE 1. Topology and control methods. (a) Topology of the grid-connected inverter system. (b) PI control method. (c) Quasi-PR control method.

Fig. 1(b) and (c) are the control block diagrams of the PI control in dq-domain, and the quasi-PR control in phase-domain, respectively. The control block diagram of the PR control in phase-domain is similar to Fig. 1(c), which only uses $G_{PR}(s)$ replacing $G_{QPR}(s)$. The controller expressions are shown as following.

$$G_v(s) = k_{p\_v} + \frac{k_{i\_v}}{s}, \quad G_{PI}(s) = k_{p\_i} + \frac{k_{i\_i}}{s} \tag{1}$$

$$G_{QPR}(s) = k_{pr} + \frac{2k_r\omega_r s}{s^2 + 2\omega_r s + \omega_0^2} \tag{2}$$

where k_{p_v}, k_{p_i} and k_{pr} are proportional coefficients; k_{i_v}, k_{i_i}, and k_r are integral coefficients; ω_r is resonance bandwidth of quasi-PR controller; the center frequency of the quasi-PR controller $\omega_0 = 2\pi f_1$; f_1 is the fundamental frequency.

$$G_{PR}(s) = G_{PI}\left(\frac{s^2+\omega_0^2}{2s}\right) = k_{pr} + \frac{2k_r s}{s^2+\omega_0^2} \tag{3}$$

Existing research shows that, after the conversion in (3), the equivalent controller, PR controller $G_{PR}(s)$ in AC system, can be obtained from the PI controller $G_{PI}(s)$ in DC system [13].

The bode plot for the transfer function of the PR controller is shown as the solid blue curve in Fig. 2. The PR control method can realize the zero steady-state error for tracking the fundamental signal.

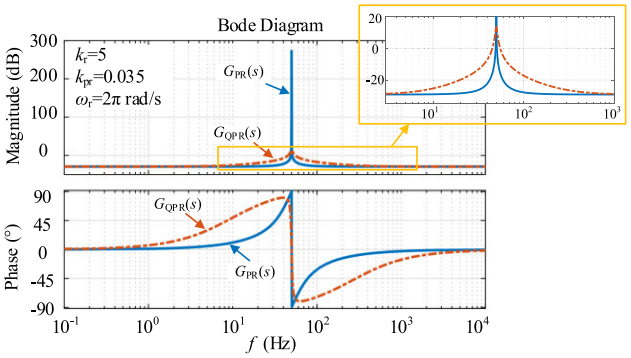

FIGURE 2. Bode diagram of transfer function in different control methods.

Considering the frequency fluctuations in the grid, a resonance bandwidth is set to make the controller can track the signal almost without steady-state error [14], which is called quasi-PR control method. According to EN 50438, the frequency fluctuation in the grid is less than ±1 Hz while the grid frequency is 50 Hz [15]. During the operation of the grid in China, the grid frequency is generally fluctuating in 49.5 Hz to 50.5 Hz. Thus, ω_r is set as 2π rad/s in this paper to meet the requirements of the control performance. The bode plot for the transfer function of the quasi-PR controller is shown with the dotted orange curve in Fig. 2. This controller can nearly realize zero steady-state error performance in the resonance bandwidth ω_r with the center frequency ω_0.

Fig. 2 shows the difference between $G_{QPR}(s)$ and $G_{PR}(s)$ exists in the relatively wide frequency range. The difference between the magnitudes of $G_{QPR}(s)$ and $G_{PR}(s)$ exists in 10 Hz to 300 Hz. What's more, the obvious difference between the phases of $G_{QPR}(s)$ and $G_{PR}(s)$ exists in 2 Hz to 1000 Hz.

The PR control method in phase-domain can be derived from the PI control method in dq-domain, thus they can make the grid-connected inverters achieve a similar performance in different coordinate systems. However, the quasi-PR control method is obtained from the PR control method through introducing resonance bandwidth, which seems make it different with the PR control method. Therefore, it is worth to be studied whether the stability of the quasi-PR controlled inverter is consistent with that of the PR and PI controlled inverters. From the view of frequency coupling admittance, this paper intends to study the stabilities of the quasi-PR, PI and PR controlled inverters.

III. FREQUENCY COUPLING ADMITTANCE MODELING OF QUASI-PR CONTROLLED INVERTER

Admittance characteristics of grid-connected inverters can be affected by control loops, control delay and frequency coupling characteristic. Thus, the admittance model of quasi-PR controlled inverter will be built considering these factors.

After a positive-sequence disturbance voltage at the disturbance frequency f_p being injected into the quasi-PR controlled inverter system. A positive-sequence disturbance response current at f_p and a negative-sequence response current at coupling frequency $f_{p1} = f_p - 2f_1$ will be generated in the output current of the grid-connected inverter due to frequency coupling characteristic. The negative-sequence response current flowing through the grid impedance will generate the negative-sequence voltage at f_{p1}. Thus, i_a and v_a can be expressed in frequency-domain as below.

$$\mathbf{I}_a[f] = \begin{cases} \mathbf{I}_1, & f = \pm f_1 \\ \mathbf{I}_p, & f = \pm f_p \\ \mathbf{I}_{p1}, & f = \pm f_{p1}, \end{cases} \quad \mathbf{V}_a[f] = \begin{cases} \mathbf{V}_1, & f = \pm f_1 \\ \mathbf{V}_p, & f = \pm f_p \\ \mathbf{V}_{p1}, & f = \pm f_{p1} \end{cases} \tag{4}$$

where $\mathbf{I}_1 = (I_1/2)e^{\pm j\varphi_{i1}}$, $\mathbf{I}_p = (I_p/2)e^{\pm j\varphi_{ip}}$, $\mathbf{I}_{p1} = (I_{p1}/2)e^{\pm j\varphi_{ip1}}$, $\mathbf{V}_1 = V_1/2$, $\mathbf{V}_p = (V_p/2)e^{\pm j\varphi_{vp}}$, $\mathbf{V}_{p1} = (V_{p1}/2)e^{\pm j\varphi_{vp1}}$; I_1, I_p, I_{p1} are the amplitudes of the currents, respectively; V_1, V_p and V_{p1}, are the amplitudes of the voltages, respectively; φ_{i1}, φ_{ip}, φ_{ip1}, φ_{vp} and φ_{vp1} are the initial phase angles of the corresponding current and voltage components, respectively.

A. MODELING OF THE VOLTAGE OUTER-LOOP

The voltage outer-loop control is the important part of the control strategy of the grid-connected inverter in Fig. 1. To accurately describe the admittance characteristics of the grid-connected inverter, the voltage outer-loop control should be considered.

According to the law of energy conservation, the power on the DC-side is equal to that on the AC-side.

$$\left(i_{pv} - sC_{dc}v_{dc}\right)v_{dc} = (v_a + sL_f i_a)\,i_a + (v_b + sL_f i_b)\,i_b + (v_c + sL_f i_c)\,i_c \tag{5}$$

The expression of v_{dc} at $f = \pm(f_p - f_1)$ can be obtained from (5) after the convolution calculation in frequency-domain.

$$v_{dc} = \frac{3\left[\mathbf{I}_1\mathbf{V}_{p1} + (sL_f\mathbf{I}_1 + \mathbf{V}_1)\,\mathbf{I}_{p1} + \left(\mathbf{V}_1^* + sL_f\mathbf{I}_1^*\right)\mathbf{I}_p + \mathbf{I}_1^*\mathbf{V}_p\right]}{i_{pv} - sC_{dc}\mathbf{V}_{dc}} \tag{6}$$

where the superscript "$*$" represents the conjugated variable; V_{dc} is the steady-state component of the DC-side voltage.

In order to simplify the expression, we can define

$$v_{\mathrm{dc}}[f] = F_{\mathrm{i}}\mathbf{I}_{\mathrm{p}} + F_{\mathrm{i1}}\mathbf{I}_{\mathrm{p1}} + F_{\mathrm{v}}\mathbf{V}_{\mathrm{p}} + F_{\mathrm{v1}}\mathbf{V}_{\mathrm{p1}} \tag{7}$$

where

$$\begin{bmatrix} F_{\mathrm{i}} & F_{\mathrm{i1}} \\ F_{\mathrm{v}} & F_{\mathrm{v1}} \end{bmatrix} = \begin{bmatrix} \dfrac{3\left(\mathbf{V}_1^* + s_2 L_{\mathrm{f}}\mathbf{I}_1^*\right)}{i_{\mathrm{pv}} - s_2 C_{\mathrm{dc}} V_{\mathrm{dc}}} & \dfrac{3\left(\mathbf{V}_1 + s_2 L_{\mathrm{f}}\mathbf{I}_1\right)}{i_{\mathrm{pv}} - s_2 C_{\mathrm{dc}} V_{\mathrm{dc}}} \\ \dfrac{3\mathbf{I}_1^*}{i_{\mathrm{pv}} - s_2 C_{\mathrm{dc}} V_{\mathrm{dc}}} & \dfrac{3\mathbf{I}_1}{i_{\mathrm{pv}} - s_2 C_{\mathrm{dc}} V_{\mathrm{dc}}} \end{bmatrix}.$$

It is defined that $s = \pm j2\pi f_{\mathrm{p}}$, $s_1 = \pm j2\pi f_1$, $s_2 = \pm(j2\pi f_{\mathrm{p}} - j2\pi f_1)$, $s_{\mathrm{p1}} = \pm(j2\pi f_{\mathrm{p}} - j4\pi f_1)$.

The reference value of the output current in dq-domain i_{dr} can be expressed as shown in below.

$$i_{\mathrm{dr}} = (v_{\mathrm{dc}} - V_{\mathrm{dc}})\, G_{\mathrm{v}}(s_2) \tag{8}$$

Submitting (6) into (8), it can be obtained

$$i_{\mathrm{dr}}[f] = \begin{cases} I_{\mathrm{dr}}, & \mathrm{dc} \\ G_{\mathrm{v}}(s_2)\, G_{\mathrm{vf}}(s_2)\, v_{\mathrm{dc}}, & f = \pm\left(f_{\mathrm{p}} - f_1\right) \end{cases} \tag{9}$$

B. MODELING OF THE PLL

Considering the disturbance, the PLL output can be expressed as $\theta_{\mathrm{PLL}}(t) = \Delta\theta_{\mathrm{PLL}}(t) + \theta_1(t)$. According to the derivation method in [5], the relationship between $\Delta\theta_{\mathrm{PLL}}$ and the disturbance voltage in PCC at $f = \pm(f_{\mathrm{p}} - f_1)$ can be obtained. The PLL transfer function $G_{\mathrm{PLL}}(s_2) = (k_{\mathrm{p\_PLL}} + k_{\mathrm{i\_PLL}}/s_2)/s_2$.

$$\Delta\theta_{\mathrm{PLL}}[f] = T_{\mathrm{p}}(s_2)\, G_{\mathrm{vf}}(s)\, \mathbf{V}_{\mathrm{p}} + T_{\mathrm{p1}}(s_2)\, G_{\mathrm{vf}}\left(s_{\mathrm{p1}}\right) \mathbf{V}_{\mathrm{p1}} \tag{10}$$

$$T_{\mathrm{p}}(s_2) = \frac{\mp jG_{\mathrm{PLL}}(s_2)}{1 + V_1 G_{\mathrm{PLL}}(s_2)},\ T_{\mathrm{p1}}(s_2) = \frac{\pm jG_{\mathrm{PLL}}(s_2)}{1 + V_1 G_{\mathrm{PLL}}(s_2)} \tag{11}$$

The output current reference value in phase A i_{ar} can be obtained by the following formula.

$$\begin{aligned} i_{\mathrm{ar}}[f] = {} & \cos(\theta_1[f]) \otimes \left(i_{\mathrm{dr}}[f] - \Delta\theta_{\mathrm{PLL}}[f] \otimes i_{\mathrm{qr}}[f]\right) \\ & - \sin(\theta_1[f]) \otimes \left(\Delta\theta_{\mathrm{PLL}}[f] \otimes i_{\mathrm{dr}}[f] + i_{\mathrm{qr}}[f]\right) \end{aligned} \tag{12}$$

where the steady-state component of i_{qr} is zero, the symbol "$\otimes$" represents a convolution calculation.

Combining (9), (10) and (12), the specific expression of i_{ar} can be derived as below.

$$i_{\mathrm{ar}}[f] = \begin{cases} 0.5\left(i_{\mathrm{dr}}[s_2] \pm jI_{\mathrm{dr}}\Delta\theta_{\mathrm{PLL}}[s_2]\right), & f = \pm f_{\mathrm{p}} \\ 0.5\left(i_{\mathrm{dr}}[s_2] \mp jI_{\mathrm{dr}}\Delta\theta_{\mathrm{PLL}}[s_2]\right), & f = \pm\left(f_{\mathrm{p}} - 2f_1\right) \end{cases} \tag{13}$$

C. MODELING OF THE QUASI-PR CONTROLLED INVERTER

According to the control block diagram shown in Fig. 1(c), the expression of the modulation signal m_1 can be obtained.

$$m_1 = \frac{\mathbf{V}_1 + j2\pi f_1 L_{\mathrm{f}}\mathbf{I}_1}{K_{\mathrm{m}} V_{\mathrm{dc}} G_{\mathrm{del}}(s_1)} \tag{14}$$

where the control delay is expressed as $G_{\mathrm{del}}(s) = e^{-1.5T_{\mathrm{s}}s}$, and T_{s} is the sampling period.

From Fig. 1(c), the relationship between the output voltage and inductor current of the grid-connected inverter can be obtained as follows.

$$sL_{\mathrm{f}}i_{\mathrm{a}} = K_{\mathrm{pwm}}G_{\mathrm{del}}v_{\mathrm{dc}} \otimes \left[(i_{\mathrm{ar}} - i_{\mathrm{a}})\, G_{\mathrm{QPR}}(s) + K_{\mathrm{f}}v_{\mathrm{a}}\right] - v_{\mathrm{a}} \tag{15}$$

Combining (5), (13) and (15), the admittance matrix of the grid-connected inverter can be calculated as

$$-\begin{bmatrix} \mathbf{I}_{\mathrm{p}} \\ \mathbf{I}_{\mathrm{p1}} \end{bmatrix} = \begin{bmatrix} Y_{11} & Y_{12} \\ Y_{21} & Y_{22} \end{bmatrix} \begin{bmatrix} \mathbf{V}_{\mathrm{p}} \\ \mathbf{V}_{\mathrm{p1}} \end{bmatrix} \tag{16}$$

The expressions of Y_{11}, Y_{12}, Y_{21} and Y_{22} in the admittance matrix are shown in (17) to (20). Those variables in (17) to (20) as shown at the bottom of the page.

$$\begin{bmatrix} J_{\mathrm{i}} \\ J_{\mathrm{i1}} \end{bmatrix} = \begin{bmatrix} -V_{\mathrm{dc}}G_{\mathrm{QPR}}(s)\, G_{\mathrm{if}}(s) \\ -V_{\mathrm{dc}}G_{\mathrm{QPR}}\left(s_{\mathrm{p1}}\right) G_{\mathrm{if}}\left(s_{\mathrm{p1}}\right) \end{bmatrix} \tag{21}$$

$$\begin{cases} H_{\mathrm{p}} = 0.5V_{\mathrm{dc}}G_{\mathrm{vf}}(s_2)\, G_{\mathrm{v}}(s_2)\, G_{\mathrm{QPR}}(s) + m_1 \\ H_{\mathrm{p1}} = 0.5V_{\mathrm{dc}}G_{\mathrm{vf}}(s_2)\, G_{\mathrm{v}}(s_2)\, G_{\mathrm{QPR}}\left(s_{\mathrm{p1}}\right) + m_1^* \end{cases} \tag{22}$$

$$Y_{11} = \frac{\left[s_{\mathrm{p1}}L_{\mathrm{f}} - \left(F_{\mathrm{i1}}H_{\mathrm{p1}} + J_{\mathrm{i1}}\right) K_{\mathrm{pwm}}G_{\mathrm{del}}\left(s_{\mathrm{p1}}\right)\right]\left[\left(F_{\mathrm{v}}H_{\mathrm{p}} + D_{\mathrm{v1}}\right) K_{\mathrm{pwm}}G_{\mathrm{del}}(s) - 1\right] + F_{\mathrm{i1}}H_{\mathrm{p}}\left(F_{\mathrm{v}}H_{\mathrm{p1}} + D_{\mathrm{v3}}\right) K_{\mathrm{pwm}}^2 G_{\mathrm{del}}(s)\, G_{\mathrm{del}}\left(s_{\mathrm{p1}}\right)}{-\left[sL_{\mathrm{f}} - \left(F_{\mathrm{i}}H_{\mathrm{p}} + J_{\mathrm{i}}\right) K_{\mathrm{pwm}}G_{\mathrm{del}}(s)\right]\left[s_{\mathrm{p1}}L_{\mathrm{f}} - \left(F_{\mathrm{i1}}H_{\mathrm{p1}} + J_{\mathrm{i1}}\right) K_{\mathrm{pwm}}G_{\mathrm{del}}\left(s_{\mathrm{p1}}\right)\right] + F_{\mathrm{i1}}H_{\mathrm{p}}F_{\mathrm{i}}H_{\mathrm{p1}}K_{\mathrm{pwm}}^2 G_{\mathrm{del}}(s)\, G_{\mathrm{del}}\left(s_{\mathrm{p1}}\right)} \tag{17}$$

$$Y_{12} = \frac{\left[s_{\mathrm{p1}}L_{\mathrm{f}} - \left(F_{\mathrm{i1}}H_{\mathrm{p1}} + J_{\mathrm{i1}}\right) K_{\mathrm{pwm}}G_{\mathrm{del}}\left(s_{\mathrm{p1}}\right)\right]\left(F_{\mathrm{v1}}H_{\mathrm{p}} + D_{\mathrm{v2}}\right) K_{\mathrm{pwm}}G_{\mathrm{del}}(s) + \left[\left(F_{\mathrm{v1}}H_{\mathrm{p1}} + D_{\mathrm{v4}}\right) K_{\mathrm{pwm}}G_{\mathrm{del}}\left(s_{\mathrm{p1}}\right) - 1\right] F_{\mathrm{i1}}H_{\mathrm{p}}K_{\mathrm{pwm}}G_{\mathrm{del}}(s)}{-\left[sL_{\mathrm{f}} - \left(F_{\mathrm{i}}H_{\mathrm{p}} + J_{\mathrm{i}}\right) K_{\mathrm{pwm}}G_{\mathrm{del}}(s)\right]\left[s_{\mathrm{p1}}L_{\mathrm{f}} - \left(F_{\mathrm{i1}}H_{\mathrm{p1}} + J_{\mathrm{i1}}\right) K_{\mathrm{pwm}}G_{\mathrm{del}}\left(s_{\mathrm{p1}}\right)\right] + F_{\mathrm{i1}}H_{\mathrm{p}}F_{\mathrm{i}}H_{\mathrm{p1}}K_{\mathrm{pwm}}^2 G_{\mathrm{del}}(s)\, G_{\mathrm{del}}\left(s_{\mathrm{p1}}\right)} \tag{18}$$

$$Y_{21} = \frac{F_{\mathrm{i}}H_{\mathrm{p1}}\left[\left(F_{\mathrm{v}}H_{\mathrm{p}} + D_{\mathrm{v1}}\right) K_{\mathrm{pwm}}G_{\mathrm{del}}(s) - 1\right] K_{\mathrm{pwm}}G_{\mathrm{del}}\left(s_{\mathrm{p1}}\right) + \left[sL_{\mathrm{f}} - \left(F_{\mathrm{i}}H_{\mathrm{p}} + J_{\mathrm{i}}\right) K_{\mathrm{pwm}}G_{\mathrm{del}}(s)\right]\left(F_{\mathrm{v}}H_{\mathrm{p1}} + D_{\mathrm{v3}}\right) K_{\mathrm{pwm}}G_{\mathrm{del}}\left(s_{\mathrm{p1}}\right)}{-\left[sL_{\mathrm{f}} - \left(F_{\mathrm{i}}H_{\mathrm{p}} + J_{\mathrm{i}}\right) K_{\mathrm{pwm}}G_{\mathrm{del}}(s)\right]\left[s_{\mathrm{p1}}L_{\mathrm{f}} - \left(F_{\mathrm{i1}}H_{\mathrm{p1}} + J_{\mathrm{i1}}\right) K_{\mathrm{pwm}}G_{\mathrm{del}}\left(s_{\mathrm{p1}}\right)\right] + F_{\mathrm{i1}}H_{\mathrm{p}}F_{\mathrm{i}}H_{\mathrm{p1}}K_{\mathrm{pwm}}^2 G_{\mathrm{del}}(s)\, G_{\mathrm{del}}\left(s_{\mathrm{p1}}\right)} \tag{19}$$

$$Y_{22} = \frac{F_{\mathrm{i}}H_{\mathrm{p1}}\left(F_{\mathrm{v1}}H_{\mathrm{p}} + D_{\mathrm{v2}}\right) K_{\mathrm{pwm}}^2 G_{\mathrm{del}}(s)\, G_{\mathrm{del}}\left(s_{\mathrm{p1}}\right) + \left[sL_{\mathrm{f}} - \left(F_{\mathrm{i}}H_{\mathrm{p}} + J_{\mathrm{i}}\right) K_{\mathrm{pwm}}G_{\mathrm{del}}(s)\right]\left[\left(F_{\mathrm{v1}}H_{\mathrm{p1}} + D_{\mathrm{v4}}\right) K_{\mathrm{pwm}}G_{\mathrm{del}}\left(s_{\mathrm{p1}}\right) - 1\right]}{-\left[sL_{\mathrm{f}} - \left(F_{\mathrm{i}}H_{\mathrm{p}} + J_{\mathrm{i}}\right) K_{\mathrm{pwm}}G_{\mathrm{del}}(s)\right]\left[s_{\mathrm{p1}}L_{\mathrm{f}} - \left(F_{\mathrm{i1}}H_{\mathrm{p1}} + J_{\mathrm{i1}}\right) K_{\mathrm{pwm}}G_{\mathrm{del}}\left(s_{\mathrm{p1}}\right)\right] + F_{\mathrm{i1}}H_{\mathrm{p}}F_{\mathrm{i}}H_{\mathrm{p1}}K_{\mathrm{pwm}}^2 G_{\mathrm{del}}(s)\, G_{\mathrm{del}}\left(s_{\mathrm{p1}}\right)} \tag{20}$$

$$\begin{cases} D_{v1} = (\pm 0.5jI_{dr}G_p(s_2)G_{QPR}(s) + K_f)V_{dc}G_{vf}(s) \\ D_{v2} = \pm 0.5jI_{dr}V_{dc}G_{vf}(s_{p1})G_{p1}(s_2)G_{QPR}(s) \\ D_{v3} = \mp 0.5jI_{dr}V_{dc}G_{vf}(s)G_p(s_2)G_{QPR}(s_{p1}) \\ D_{v4} = (\mp 0.5jI_{dr}G_{p1}(s_2)G_{QPR}(s_{p1}) \\ \qquad + K_f)V_{dc}G_{vf}(s_{p1}) \end{cases} \quad (23)$$

IV. COMPARISON OF ADMITTANCE CHARACTERISTICS OF THE QUASI-PR, PI AND PR CONTROLLED INVERTERS

The parameters of the quasi-PR controlled inverter studied in this paper are shown in Table 1. In order to verify the correctness of the established admittance model, an admittance measurement platform was established in Matlab/Simulink. The admittance measurement results of the quasi-PR controlled inverter are shown in Fig. 3. The solid red line indicates the established frequency coupling admittance model of the quasi-PR controlled inverter, and the red circle represents the admittance measurement result. It can be seen from Fig. 3 that the admittance measurement results essentially agree with the established frequency coupling admittance model, which proves the correctness of the established frequency coupling admittance model of the quasi-PR controlled inverter.

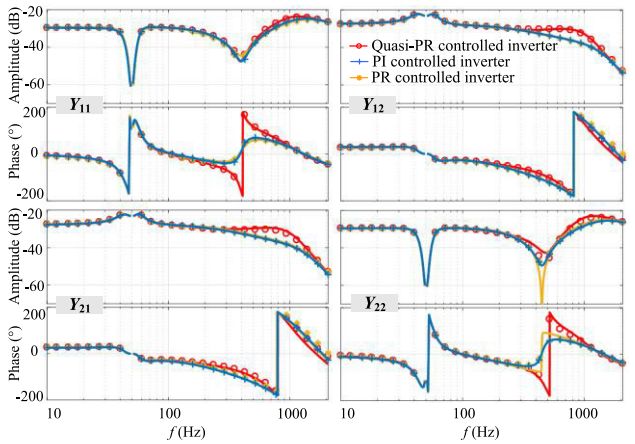

FIGURE 3. Admittance characteristic curves of the grid-connected inverter under these three control methods.

The frequency coupling admittance models of the PI and PR controlled inverters are shown as (24)-(25).

$$-\begin{bmatrix} \mathbf{I}_p \\ \mathbf{I}_{p1} \end{bmatrix} = \begin{bmatrix} Y_{11\_PI} & Y_{12\_PI} \\ Y_{21\_PI} & Y_{22\_PI} \end{bmatrix} \begin{bmatrix} \mathbf{V}_p \\ \mathbf{V}_{p1} \end{bmatrix} \quad (24)$$

$$-\begin{bmatrix} \mathbf{I}_p \\ \mathbf{I}_{p1} \end{bmatrix} = \begin{bmatrix} Y_{11\_PR} & Y_{12\_PR} \\ Y_{21\_PR} & Y_{22\_PR} \end{bmatrix} \begin{bmatrix} \mathbf{V}_p \\ \mathbf{V}_{p1} \end{bmatrix} \quad (25)$$

In order to compare and analyze the admittance characteristics of the quasi-PR, PI and PR controlled inverters more conveniently, the admittance model and measurement results of the PI and PR controlled inverters also are drawn in Fig. 3. The admittance modeling of the PI controlled inverter has been studied a lot [5], in addition, the frequency coupling admittance model of the PR controlled inverter only need replace the $G_{QPR}(s)$ in the established admittance model of the PR controlled inverter with $G_{PR}(s)$. Thus, the frequency coupling admittance models of the PI and PR controlled inverters will not be deduced in this paper.

TABLE 1. Parameters of the Quasi-PR controlled inverter.

Symbol	Quantity	Values
L_f	filter inductance	3 mH
C_f	filter capacitor	20 μF
R_d	damping resistance of filter capacitor	1.5 Ω
v_{ref}	DC-side voltage	700 V
V_1	grid voltage	311 V
f_1	fundamental frequency	50 Hz
K_{pwm}	modulation coefficient	0.5
i_{dc}	the DC-side current	14.29 A
T_s	the sampling period	5×10^{-5} s
k_{p_PLL}	proportional coefficient in $G_{PLL}(s)$	0.2659
k_{i_PLL}	integral coefficient in $G_{PLL}(s)$	10.9988
ω_r	resonance bandwidth of QPR controller	2π rad/s
k_{pr}	proportional coefficient of QPR controller	0.035
k_r	integral coefficient of QPR controller	5
k_{p_v}	proportional coefficient in $G_v(s)$	8.3398
k_{i_v}	integral coefficient in $G_v(s)$	698.5
ω_{vf}	the cut-off frequency of the sampling filters for the voltage	2π·4000 rad/s
ω_{if}	the cut-off frequency of the sampling filters for the current	2π·4000 rad/s
K_f	voltage feed forward coefficient	1/350

In Fig. 3, the frequency coupling admittance model of the PI controlled inverter is represented by a solid blue line, and the admittance measurement result is represented by the blue cross; the frequency coupling admittance model of the PR controlled inverter is represented by a solid yellow line, and the admittance measurement result is represented by the yellow star. Their simulation parameters are consistent with that of the quasi-PR controlled inverter.

According to the comparison of the three admittance models, the admittance characteristics of the PR controlled inverter is very similar to that of the PI controlled inverter. However, the quasi-PR controlled inverter is quite different from that of the PI and PR controlled inverters.

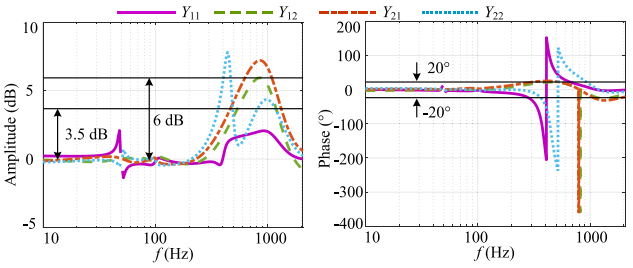

FIGURE 4. Admittance differences between quasi-PR and PI controlled inverters.

To describe this difference clearly, the admittance differences between the quasi-PR and PI controlled inverters are shown in Fig. 4. The different colors and curves are used to present the admittance differences of Y_{11}, Y_{12}, Y_{21}, and Y_{22}. In the frequency areas 350 Hz to 1300 Hz, the amplitude difference is larger than 3.5 dB. In the frequency areas 400 Hz to 500 Hz and 600 Hz to 1100 Hz, the amplitude difference is

larger than 6 dB which indicates the amplitude of the quasi-PR controlled inverter is more than twice as large as that of the PI controlled inverter. In 250 Hz to 2000 Hz, the phase difference is larger than 20 degrees.

Therefore, the admittance differences between the quasi-PR and PI controlled inverters are quite large.

In order to further explore the factor caused the above admittance differences, we try to focus on the only different parameter ω_r between the PI and quasi-PR controllers. The admittance characteristics of the quasi-PR controlled inverter when the ω_r is changed are observed and their admittance characteristic differences are compared as shown in Fig. 5.

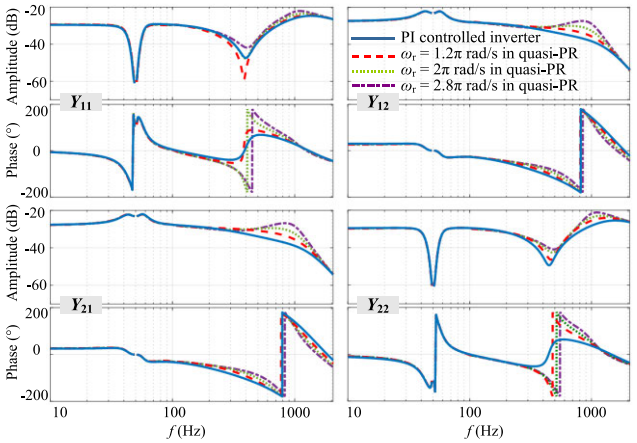

FIGURE 5. Admittance characteristic curves when ω_r changes.

In Fig. 5, the change of ω_r has a great impact on admittance characteristics in the mid-high frequency areas. As ω_r increases, the admittance peaks become sharper. The smaller the ω_r, the closer the admittance characteristics of the quasi-PR and PI controlled inverters.

Thus, the resonance bandwidth of the quasi-PR controller is an important factor that causes differences in admittance characteristics of the grid-connected inverters under the quasi-PR and PI control methods.

V. COMPARATIVE ANALYSES OF SYSTEM STABILITY

Based on the established frequency coupling admittance model and generalized Nyquist criterion, the influence of the grid impedance, inverter output power P_s and the outer-loop bandwidth BW_v on system stability are studied and the system stabilities for the quasi-PR, PI and PR controlled inverters are compared. The equivalent return matrix of the grid-connected inverter system in Fig. 1(a) can be defined as below.

$$L = Z_g \cdot Y_{inv} = \begin{bmatrix} Z_{g11} \cdot Y_{11} & Z_{g11} \cdot Y_{12} \\ Z_{g22} \cdot Y_{21} & Z_{g22} \cdot Y_{22} \end{bmatrix} \tag{26}$$

where $Z_{g11} = Z_g(s)$, $Z_{g22} = Z_g(s - j4\pi f_1)$.

The filter capacitor branch is not included in the control of the grid-connected inverter. Thus, the filter capacitor branch can be regarded as a part of the grid impedance:

$$Z_g(s) = \frac{(sL_g + R_g)\left[R_f + 1/(sC_f)\right]}{sL_g + R_g + R_f + 1/(sC_f)} \tag{27}$$

According to (26), λ_1 and λ_2 are defined as the eigenvalues of the return matrix. The system stability is analyzed by the Nyquist diagrams of λ_1 and λ_2 which are indicated by the solid and dotted line, respectively. $a = 1$, $b = -(Z_{g11}Y_{11} + Z_{g22}Y_{22})$, $c = Z_{g11}Z_{g22}(Y_{11}Y_{22} - Y_{12}Y_{21})$.

$$\lambda_1 = \frac{-b + \sqrt{b^2 - 4ac}}{2a}, \quad \lambda_1 = \frac{-b - \sqrt{b^2 - 4ac}}{2a} \tag{28}$$

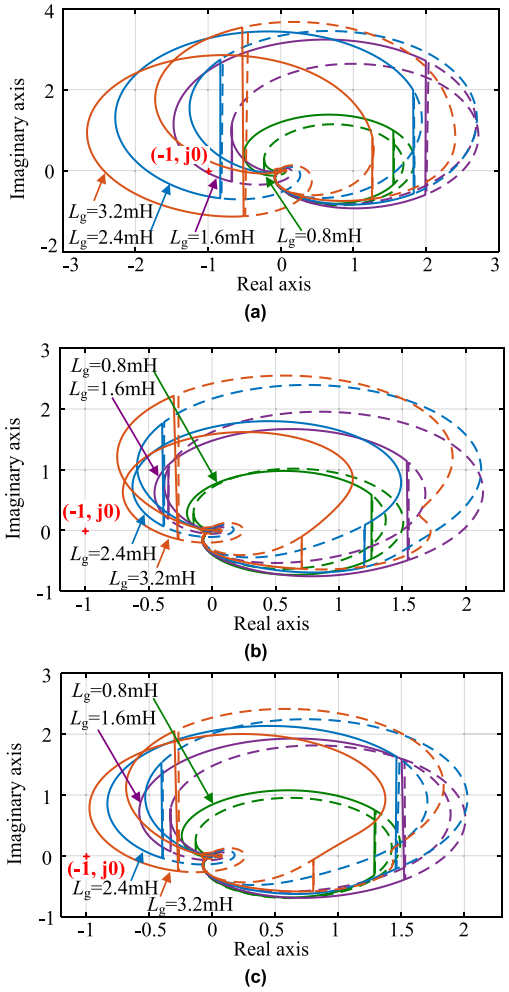

FIGURE 6. The Nyquist diagram when L_g is changed. (a) The quasi-PR controlled inverter. (b)The PI controlled inverter. (c) The PR controlled inverter.

A. THE EFFECTS OF THE GRID IMPEDANCE ON SYSTEM STABILITY

To comparatively study system stability when L_g is changed, the Nyquist diagrams in Fig. 6 are analyzed. In Fig. 6(a), when the L_g is 1.6 mH, 2.4 mH, or 3.2 mH, the Nyquist curves of the quasi-PR controlled inverter have surrounded the point (–1, j0), which indicates the system is unstable. As shown in Fig. 6(b) and Fig. 6(c), the Nyquist curves of the PI and PR controlled inverters do not surround the point (–1, j0) even the L_g is 3.2 mH, which indicates the systems can remain stable.

Therefore, under the same conditions, the PI and PR controlled inverters have a similar system stability while the

quasi-PR controlled inverter is more sensitive to the weak grid.

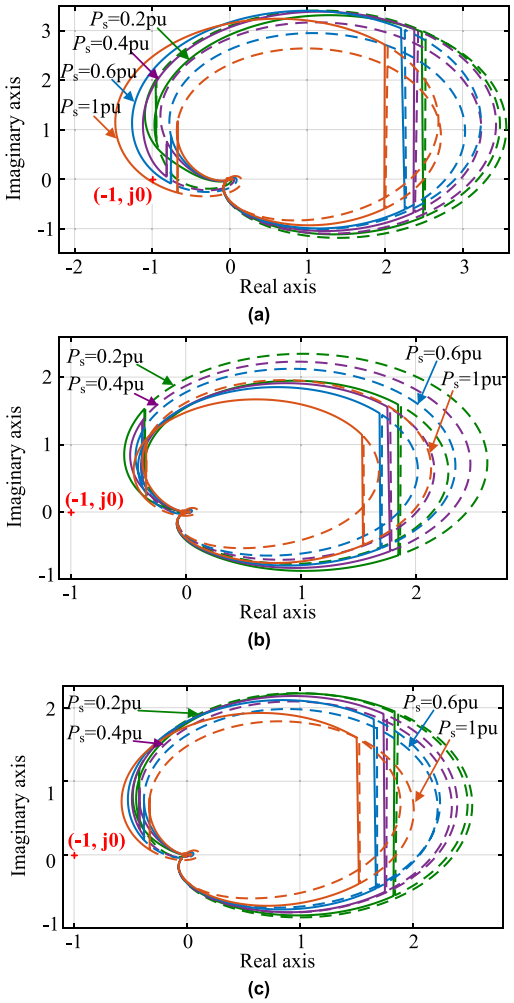

FIGURE 7. The Nyquist diagram when P_S is changed. (a) The quasi-PR controlled inverter. (b)The PI controlled inverter. (c) The PR controlled inverter.

B. THE EFFECTS OF THE INVERTER OUTPUT POWER ON SYSTEM STABILITY

The Nyquist diagrams when the P_s is 1 pu, 0.6 pu, 0.4 pu, or 0.2 pu in Fig. 7 are analyzed while L_g is 1.6 mH. The Nyquist curves in Fig. 7(b) and (c) are not surrounds the point (–1, j0) and the systems are stable. However, the Nyquist curve in Fig. 7(a) surrounds the point (–1, j0) when the P_s is 1 pu and the quasi-PR controlled inverter system is unstable.

Thus, under the same operating conditions, compared with the PI and PR controlled inverters, the quasi-PR controlled inverter is more sensitive to high P_s.

C. THE EFFECTS OF THE OUTER-LOOP BANDWIDTH ON SYSTEM STABILITY

In order to study the effects of the outer-loop bandwidth on system stability, while L_g is 0.8 mH, the Nyquist diagrams when the BW_v is changed in Fig. 8 are analyzed.

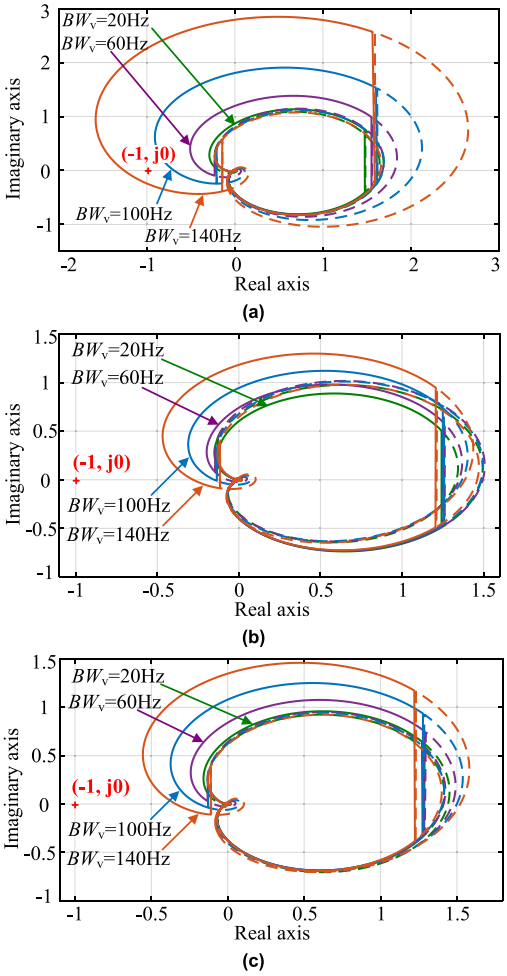

FIGURE 8. Nyquist diagram when BW_v is changed. (a) The quasi-PR controlled inverter. (b)The PI controlled inverter. (c) The PR controlled inverter.

As shown in Fig. 8(a), when BW_v is 140 Hz, the Nyquist curve of the quasi-PR controlled inverter has surrounded the point (–1, j0), which indicates the system is unstable. In Fig. 8(b) and Fig. 8(c), the Nyquist curves of the PI and PR controlled inverters do not surround the point (–1, j0), which indicates the systems are stable.

Thus, under the same operate condition, to achieve the same system stability, the outer-loop bandwidth of the quasi-PR controlled inverter should be designed narrower than that of the PI and PR controlled inverters.

D. THE EFFECTS OF THE RESONANCE BANDWIDTH ON SYSTEM STABILITY

To analyze the system stability when ω_r is changed, the Nyquist diagram in Fig. 9 is studied while L_g is 1.6 mH and P_s is 0.6 pu.

In Fig. 9, when ω_r is increased to 2.8π rad/s, the Nyquist curve of the quasi-PR controlled inverter has surrounded the point (–1, j0), which indicates that the system is unstable. Therefore, with the increasing of ω_r, the quasi-PR controlled inverter system tends to be unstable.

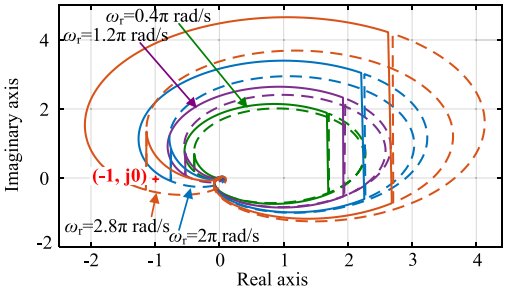

FIGURE 9. Nyquist diagram of quasi-PR controlled inverter when ω_r is changed.

From the above analysis, it is can be seen that the stabilities of the PI and PR controlled inverters are similar while the stability of the quasi-PR controlled inverter is worse than that of the PI and PR controlled inverters.

In the quasi-PR controlled inverter system, the ω_r is an important factor that affects the system stability. To reduce the impact on system stability, the ω_r should be set as small as possible in the area which can meet the control requirement.

VI. EXPERIMENTAL RESULTS

To verify the correctness of the above analysis, experiments were carried out on the controller hardware-in-the-loop experimental platform, as shown in Fig. 10. Experimental parameters are consistent with Section V.

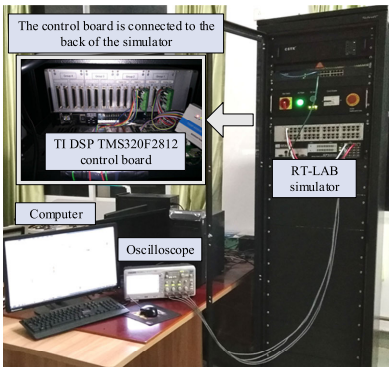

FIGURE 10. The HIL experimental platform.

The design process of the PR controller is introduced below. Firstly, it can be defined that

$$\frac{y(s)}{u(s)} = G_{PR}(s), \quad \frac{y_1(s)}{u(s)} = \frac{2k_r s}{s^2 + \omega_0^2} \tag{29}$$

$y_1(s)$ can be expressed as shown below.

$$y_1(s) = (2k_r u(s) - v(s))/s \tag{30}$$

where $v(s) = \omega_0^2 y_1(s)/s$.

Combining (3), (29) and (30), $y(s)$ can be expressed as (31) and the block diagram shown is shown in Fig. 11.

$$y(s) = k_{pr} u(s) + (2k_r u(s) - v(s))\frac{1}{s} \tag{31}$$

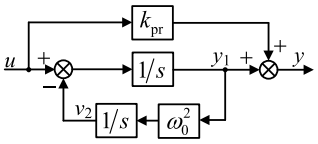

FIGURE 11. The decomposition block diagram of the $G_{PR}(s)$.

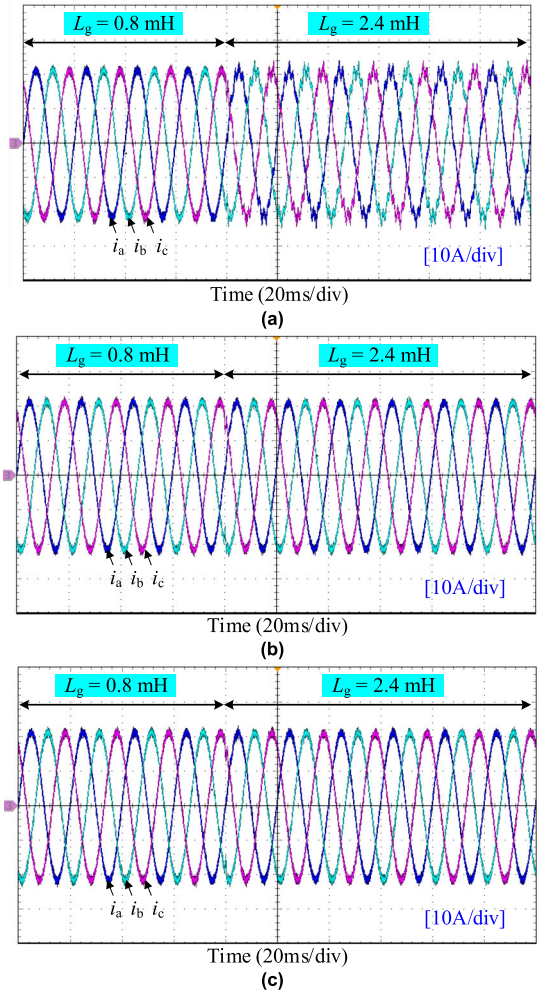

FIGURE 12. The experimental results when L_g is increased from 0.8 mH to 2.4 mH. (a) The quasi-PR controlled inverter. (b)The PI controlled inverter. (c) The PR controlled inverter.

After discretizing, (31) is shown as below.

$$\begin{cases} y(k) = y(k-1) + T_P\left[k_{pr}u(k-1) + \left(2k_r u(k-1) - v(k-1)\right)\right] \\ v(k) = v(k-1) + \omega_0^2 T_P y(k) \end{cases} \tag{32}$$

where T_P is PWM carrier period.

According to the discrete expressions of y, $G_{PR}(s)$ can be realized in the TI DSP TMS320F2812 control board.

A. THE EFFECTS OF GRID IMPEDANCE ON SYSTEM STABILITY

Fig. 12 shows the experimental results when L_g is increased from 0.8 mH to 2.4 mH.

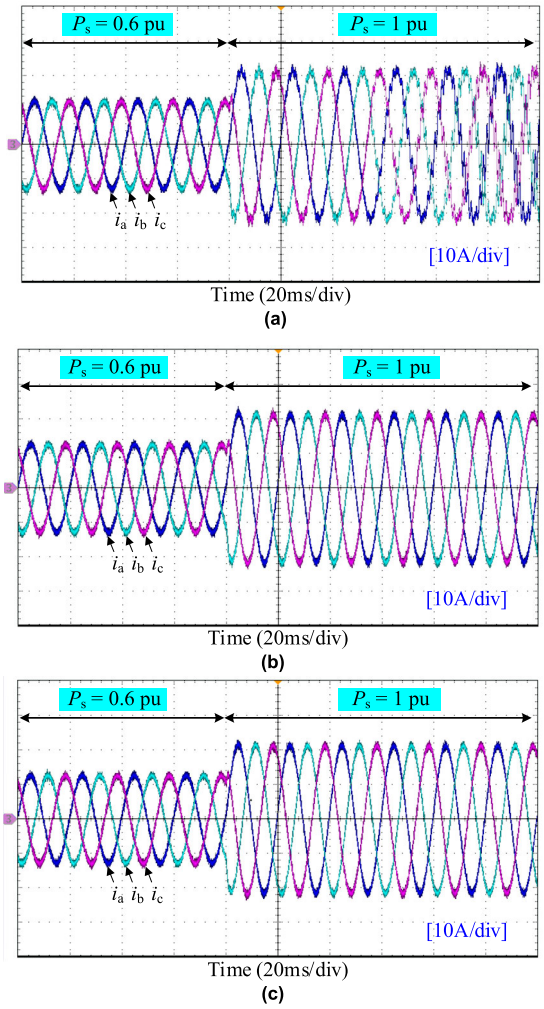

FIGURE 13. The experimental results when P_S is increased from 0.6 pu to 1 pu. (a) The quasi-PR controlled inverter. (b) The PI controlled inverter. (c) The PR controlled inverter.

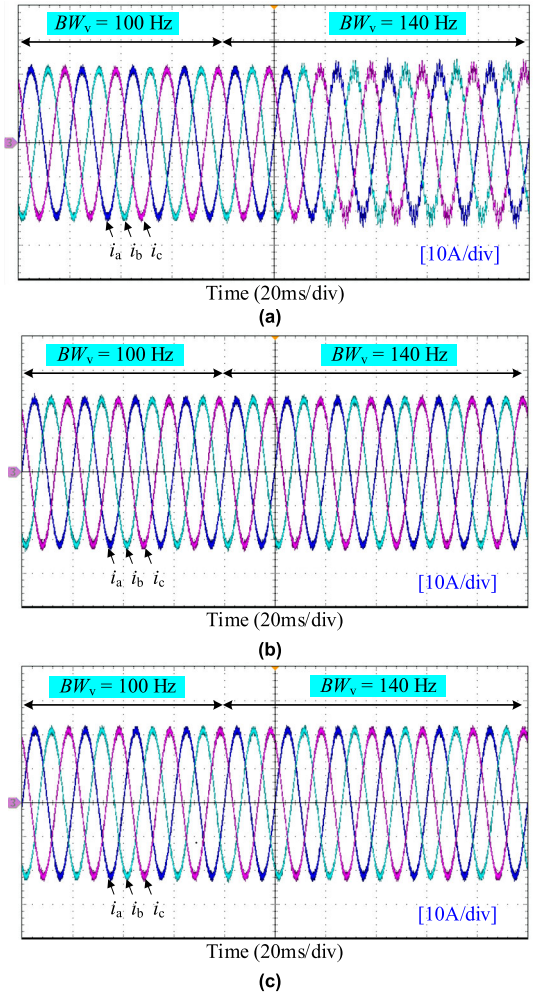

FIGURE 14. The experimental results when BW_V is increased from 100 Hz to 140 Hz. (a) The quasi-PR controlled inverter. (b) The PI controlled inverter. (c) The PR controlled inverter.

When L_g is increased to 2.4 mH, the quasi-PR controlled inverter is unstable while the PI and PR controlled inverters can still maintain stable. Therefore, under the same operating conditions, the PI and PR controlled inverters have a similar system stability, but the quasi-PR controlled inverter is more sensitive to the weak grid.

B. THE EFFECTS OF THE INVERTER OUTPUT POWER ON SYSTEM STABILITY

The experimental results when P_s is changed are shown in Fig. 13. When P_s is increased from 0.6 pu to 1 pu, the quasi-PR controlled inverter is unstable while the PI and PR controlled inverters can keep stable.

Thus, under the same operating conditions, compared with PI and PR controlled inverters, the quasi-PR controlled inverter is more sensitive to high inverter output power.

C. THE EFFECTS OF THE OUTER-LOOP BANDWIDTH ON SYSTEM STABILITY

The experimental results reflecting the influence of BW_v are shown in Fig. 14. When BW_v is increased from 100 Hz to 140 Hz, the quasi-PR controlled inverter is unstable while the PI and PR controlled inverters can still maintain stable.

Therefore, under the same conditions, BW_v of the quasi-PR controlled inverter should be designed narrower than that of the PI and PR controlled inverters to keep the system stable.

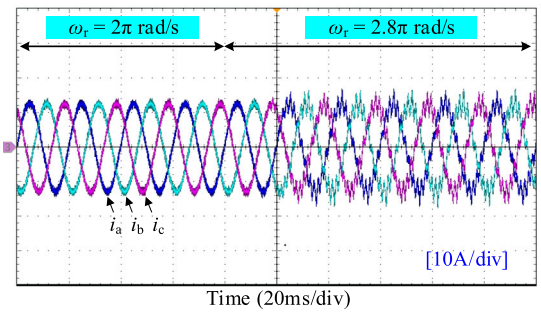

FIGURE 15. The experimental results of the quasi-PR controlled inverter when ω_r is increased from 2π rad/s to 2.8π rad/s.

D. THE EFFECTS OF THE RESONANCE BANDWIDTH ON SYSTEM STABILITY

The experimental result when ω_r is changed is shown in Fig. 15. When ω_r is increased from 2π rad/s to 2.8π rad/s, the quasi-PR controlled inverter system oscillates. The experimental result is consistent with the theoretical analysis in Fig. 9.

Therefore, the stability of the quasi-PR controlled inverter is also affected by the resonance bandwidth of the quasi-PR controller. The theoretical analysis is verified by the experimental results.

VII. CONCLUSION

In this paper, considering the influence of frequency coupling characteristic, a frequency coupling admittance model of the quasi-PR controlled inverter is established, and its stabilities are compared with the PI and PR controlled inverters. Following conclusions are drawn:

1) Admittance characteristics of the PI and PR controlled inverters are similar while the quasi-PR controlled inverter is quite different: the amplitude of the quasi-PR controlled inverter is larger than that of the PI controlled inverter and the phase difference between the two inverters is obvious in the mid-high frequency areas.
2) The resonance bandwidth of the quasi-PR controller is an important factor that causes the mentioned admittance difference. With the increasing of the resonance bandwidth, the quasi-PR controlled inverter system tends to be unstable. To reduce the impact on system stability, the resonance bandwidth should be set as small as possible in the area which can meet the control requirement.
3) The admittance difference has a great impact on system stability. Compared with the PI and PR controlled inverters, the quasi-PR controlled inverter is more sensitive to weak grid and high inverter output power. To achieve the same system stability, the outer-loop bandwidth of the quasi-PR controlled inverter should be designed narrower than that of the PI and PR controlled inverters.

REFERENCES

[1] L. Yang, Y. Chen, A. Luo, and K. Huai, "Stability enhancement for parallel grid-connected inverters by improved notch filter," *IEEE Access*, vol. 7, pp. 65667–65678, 2019.

[2] A. A. Hadi, C. A. S. Silva, E. Hossain, and R. Challoo, "Algorithm for demand response to maximize the penetration of renewable energy," *IEEE Access*, vol. 8, pp. 55279–55288, 2020.

[3] Z. Xie, W. Wu, Y. Chen, and W. Gong, "Admittance-based stability comparative analysis of grid-connected inverters with direct power control and closed-loop current control," *IEEE Trans. Ind. Electron.*, vol. 68, no. 9, pp. 8333–8344, Sep. 2021.

[4] W. Wu, Y. Chen, L. Zhou, X. Zhou, L. Yang, Y. Dong, Z. Xie, and A. Luo, "A virtual phase-lead impedance stability control strategy for the maritime VSC–HVDC system," *IEEE Trans. Ind. Informat.*, vol. 14, no. 12, pp. 5475–5486, Dec. 2018.

[5] M. Cespedes and J. Sun, "Impedance modeling and analysis of grid-connected voltage-source converters," *IEEE Trans. Power Electron.*, vol. 29, no. 3, pp. 1254–1261, Mar. 2014.

[6] K. M. Alawasa and Y. A.-R.-I. Mohamed, "A simple approach to damp SSR in series-compensated systems via reshaping the output admittance of a nearby VSC-based system," *IEEE Trans. Ind. Electron.*, vol. 62, no. 5, pp. 2673–2682, May 2015.

[7] J. Yin, S. Duan, and B. Liu, "Stability analysis of grid-connected inverter with LCL filter adopting a digital single-loop controller with inherent damping characteristic," *IEEE Trans. Ind. Informat.*, vol. 9, no. 2, pp. 1104–1112, May 2013.

[8] S. Eren, M. Pahlevani, A. Bakhshai, and P. Jain, "A digital current control technique for grid-connected AC/DC converters used for energy storage systems," *IEEE Trans. Power Electron.*, vol. 32, no. 5, pp. 3970–3988, May 2017.

[9] L. Wang, M. Wang, B. Guo, Z. Wang, D. Wang, and Y. Li, "A loading control strategy for electric load simulators based on proportional resonant control," *IEEE Trans. Ind. Electron.*, vol. 65, no. 6, pp. 4608–4618, Jun. 2018.

[10] Z. Xie, Y. Chen, W. Wu, Y. Xu, H. Wang, J. Guo, and A. Luo, "Modeling and control parameters design for grid-connected inverter system considering the effect of PLL and grid impedance," *IEEE Access*, vol. 8, pp. 40474–40484, 2020.

[11] W. Wu, L. Zhou, Y. Chen, A. Luo, Y. Dong, X. Zhou, Q. Xu, L. Yang, and J. M. Guerrero, "Sequence-impedance-based stability comparison between VSGs and traditional grid-connected inverters," *IEEE Trans. Power Electron.*, vol. 34, no. 1, pp. 46–52, Jan. 2019.

[12] Q. Zhao and Y. Ye, "A PIMR-type repetitive control for a grid-tied inverter: Structure, analysis, and design," *IEEE Trans. Power Electron.*, vol. 33, no. 3, pp. 2730–2739, Mar. 2018.

[13] D. N. Zmood and D. G. Holmes, "Stationary frame current regulation of PWM inverters with zero steady-state error," *IEEE Trans. Power Electron.*, vol. 18, no. 3, pp. 814–822, May 2003.

[14] G. Shen, X. Zhu, J. Zhang, and D. Xu, "A new feedback method for Pr current control of LCL-filter-based grid-connected inverter," *IEEE Trans. Ind. Electron.*, vol. 57, no. 6, pp. 2033–2041, Jun. 2010.

[15] *Requirements for the Connection of Micro Generators in Parallel With Public Low-Voltage Distribution Networks*, document EN 50438, 2008.

[16] T. Ye, N. Dai, C.-S. Lam, M.-C. Wong, and J. M. Guerrero, "Analysis, design, and implementation of a quasi-proportional-resonant controller for a multifunctional capacitive-coupling grid-connected inverter," *IEEE Trans. Ind. Appl.*, vol. 52, no. 5, pp. 4269–4280, Sep. 2016.

[17] H. Komurcugil, N. Altin, S. Ozdemir, and I. Sefa, "Lyapunov-function and proportional-resonant-based control strategy for single-phase grid-connected VSI with LCL filter," *IEEE Trans. Ind. Electron.*, vol. 63, no. 5, pp. 2838–2849, May 2016.

[18] J. Xia, Y. Guo, X. Zhang, J. Jatskevich, and N. Amiri, "Robust control strategy design for single-phase grid-connected converters under system perturbations," *IEEE Trans. Ind. Electron.*, vol. 66, no. 11, pp. 8892–8901, Nov. 2019.

[19] D. G. Holmes, T. A. Lipo, B. P. McGrath, and W. Y. Kong, "Optimized design of stationary frame three phase AC current regulators," *IEEE Trans. Power Electron.*, vol. 24, no. 11, pp. 2417–2426, Nov. 2009.

[20] L. Dong, J. Kong, J. Feng, and Y. Zhang, "Subsynchronous resonance Mitigation for series compensation transmission system of DFIG based on Pr control," in *Proc. IEEE 10th Int. Symp. Power Electron. for Distrib. Gener. Syst. (PEDG)*, Xi'an, China, Jun. 2019, pp. 734–738.

[21] S. Zhang, S. Jiang, X. Lu, B. Ge, and F. Z. Peng, "Resonance issues and damping techniques for grid-connected inverters with long transmission cable," *IEEE Trans. Power Electron.*, vol. 29, no. 1, pp. 110–120, Jan. 2014.

[22] X. Xu, M. Zhu, C. Hou, and X. Cai, "Impedance readjusting method of grid-connected inverter cluster with Pr control strategy," in *Proc. 14th IEEE Conf. Ind. Electron. Appl. (ICIEA)*, Xi'an, China, Jun. 2019, pp. 1342–1347.

[23] I. Vieto, X. Du, H. Nian, and J. Sun, "Frequency-domain coupling in two-level VSC small-signal dynamics," in *Proc. IEEE 18th Workshop Control Modeling Power Electron. (COMPEL)*, New York, NY, USA, Jul. 2017, pp. 1–8.

[24] Y. Zhou, H. Hu, X. Yang, J. Yang, Z. He, and S. Gao, "Low frequency oscillation traceability and suppression in railway electrification systems," *IEEE Trans. Ind. Appl.*, vol. 55, no. 6, pp. 7699–7711, Nov. 2019.

[25] J. Man, X. Xie, S. Xu, C. Zou, and C. Yin, "Frequency-coupling impedance model based analysis of a high-frequency resonance incident in an actual MMC-HVDC system," *IEEE Trans. Power Del.*, vol. 35, no. 6, pp. 2963–2971, Dec. 2020.
[26] A. Manoloiu, H. A. Pereira, R. Teodorescu, M. Bongiorno, M. Eremia, and S. R. Silva, "Comparison of Pi and Pr current controllers applied on two-level VSC-HVDC transmission system," in *Proc. IEEE Eindhoven PowerTech*, Eindhoven, The Netherlands, Jun. 2015, pp. 1–5.

ZHIWEI XIE was born in Hunan, China, in 1994. She received the Ph.D. degree in electrical engineering from Hunan University, Changsha, China, in 2021.

Her research interests include power electronics converter and distributed generation.

YANDONG CHEN (Senior Member, IEEE) was born in Hunan, China, in 1979. He received the B.S. and M.S. degrees in instrument science and technology and the Ph.D. degree in electrical engineering from Hunan University, Changsha, China, in 2003, 2006, and 2014, respectively.

He has been a Professor with the College of Electrical and Information Engineering, Hunan University. His research interests include power electronics for microgrid, distributed generation, power supply, and energy storage. He is a Senior Member of the IEEE PES and PELS. He was a recipient of the 2014 National Technological Invention Awards of China, and the 2014 WIPO-SIPO Award for Chinese Outstanding Patented Invention.

WENHUA WU (Member, IEEE) was born in Hunan, China, in 1991. He received the B.S. and Ph.D. degrees in electrical engineering from Hunan University, Changsha, China, in 2014 and 2019, respectively.

He is currently a Postdoctoral Researcher in electrical engineering with Hunan University. His research interests include power electronics, and distributed power systems.

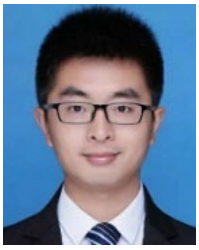

YICHAO WANG was born in Loudi, Hunan, China, in 1988. He received the bachelor's degree from the Changsha University of Science and Technology, Changsha, China, in 2010, and the Ph.D. degree from Hunan University, Changsha, in 2015.

Since 2017, he has been a Senior Engineer with State Grid Hunan Electric Power Company Ltd., Economical and Technical Research Institute, Changsha. His current research interests include power quality control, new energy power generation, and power electronics applications in power systems.

WENLAN GONG was born in Guangxi, China, in 1992. She received the M.S. degree from the College of Electrical and Information Engineering, Hunan University, Changsha, China, in 2019.

She is currently working with Electric Power Research Institute of Guangxi Power Grid Company Ltd., Nanning, China. Her research interests include power electronics converter, reactive power compensation, and distributed generation.

JOSEP M. GUERRERO (Fellow, IEEE) received the B.S. degree in telecommunications engineering, the M.S. degree in electronics engineering, and the Ph.D. degree in power electronics from the Technical University of Catalonia, Barcelona, in 1997, 2000, and 2003, respectively.

Since 2011, he has been a Full Professor with the Department of Energy Technology, Aalborg University, Denmark. His research interests include power electronics, distributed energy-storage, and microgrids. He was elevated as the IEEE Fellow for his contributions on distributed power systems and microgrids, in 2015. He is an Associate Editor of the IEEE TRANSACTIONS ON POWER ELECTRONICS, the IEEE TRANSACTIONS ON INDUSTRIAL ELECTRONICS, and the *IEEE Industrial Electronics Magazine*, and an Editor of the IEEE TRANSACTIONS ON SMART GRID and IEEE TRANSACTIONS ON ENERGY CONVERSION. He was awarded by Thomson Reuters as a Highly Cited Researcher, in 2014, 2015, and 2016.